Progress In Electromagnetics Research, Vol. 132, 159–175, 2012

TRANSIENT RESISTANCE ANALYSIS OF LARGE GROUNDING SYSTEMS USING THE FDTD METHOD

R. Xiong[1, *], B. Chen[1], J.-J. Han[2], Y.-Y. Qiu[1], W. Yang[3], and Q. Ning[1]

[1]National Key Laboratory on Electromagnetic Environment and Electro-optical Engineering, PLA University of Science and Technology, Nanjing, Jiangsu 210007, China

[2]Xian Architectural Research Institute, Xian, Shaanxi 710032, China

[3]Engineering and Design Institute, Chengdu Military Area of PLA, Kunming, Yunnan 650222, China

Abstract—In this work, a new method has been proposed for the finite-difference time-domain (FDTD) analysis of the transient grounding resistance (TGR) of large grounding systems. To calculate the TGR, a coarse grid is occupied to model the earthing conductor, the convolution PML (CPML) is chose to truncate the computational domain, and the parallel implementation is involved to overcome the memory limit of the serial FDTD. With this model, the effect of the earthing conductor number and topology structure, the buried depth, and the ground permittivity and conductivity on the TGR is tested to find an optimized program to decrease the TGR of the lightning protection grounding systems.

1. INTRODUCTION

Spacious grounding system with complex configuration of earthing conductors is often a part of the lightning protection system [1–5]. When lightning strikes, large currents flow before dissipating in the ground and the voltage on the equipment is mainly determined by the resistance of the grounding systems [6–8]. The voltage may result in damage to the equipments and cause serious accidents, such as failure of electrical transmission and danger to personnel working nearby.

Received 26 August 2012, Accepted 17 September 2012, Scheduled 27 September 2012

* Corresponding author: Run Xiong (xiongrun1983@sina.com).

Therefore, it is important to analyze the transient behavior of the grounding systems in terms of the transient grounding resistance (TGR), in order to understand all the phases of such accidents and to apply the results to improve the behavior of the lightning protection grounding systems.

The finite-difference time-domain (FDTD) method has been widely applied in solving many types of electromagnetic problems [9–17], and it has been used to investigate the transient characteristics of grounding systems since 2001 [18, 19]. However, it is difficult to use the general FDTD method to calculate the TGR of the engineering practice grounding systems, because the engineering used electrode is electrically small compared with the dimension of the grounding system. Additionally, the lightning current last a long time, and the late-time reflection of the absorbing boundary condition may introduce huge errors to the TGR.

In this paper, a novel method has been proposed for the FDTD analysis of the transient behavior of large grounding systems. The coarse FDTD grid is occupied to simulate the earthing conductor [20], the convolution perfectly matched layer (CPML) is used to absorb the late-time reflection [21, 22], and the parallel implement is involved to overcome the memory limit of the serial processor [23–27]. With the proposed method, the effect of the electrode number, topology structure, buried depth, and the ground permittivity and conductivity are tested to find an optimized program for large grounding systems.

2. THE METHOD FOR THE FDTD ANALYSIS OF THE TGR OF LARGE GROUNDING SYSTEMS

In this section, a new method has been proposed for the FDTD analysis of the TGR of large grounding systems. Firstly, the TGR calculation model is introduced, and then the coarse FDTD grid is occupied to simulate the earthing conductor. Thirdly, the absorbing boundary is chose to truncate the computational domain. Finally, the parallel implementation is introduced to overcome the memory limit of the serial FDTD.

2.1. The TGR Calculation Model

To calculate the TGR, a grounding model is adopted as shown in Fig. 1, where the earth is used as the return path [19]. A remote electrode, which is 2.5 m ($hr = 2.5$ m) in depth, is used to permit passing current into the ground. The lifting line, connecting line and remote current electrode are all round steel with a diameter of 0.025 m. The lightning

pulse current, which can be expressed by the double-exponential pulse, is injected from the lifting line at the point 0.25 m above the ground surface

$$I(t) = kI_0\left(e^{-\alpha t} - e^{-\beta t}\right) \tag{1}$$

where $\alpha = 3.7618 \times 10^4\,\mathrm{s}^{-1}$, $\beta = 1.13643 \times 10^7\,\mathrm{s}^{-1}$, $k = 1.02$, $I_0 = 5.4 \times 10^3$ A. The effective frequency spectrum of the pulse ranges from DC to 10 MHz. It is assumed that the ground has a constant constitutive parameter, and the relative permittivity of the ground is set as 9.0 and the conductivity is 0.004 S/m.

The TGR is defined as a ratio of the transient voltage to the transient current

$$R_t = V_t / I_t \tag{2}$$

where I_t is the transient current flowing through grounding conductor, which can be defined from the Ampere's Law

$$\begin{aligned} I_t \;=\; & \left[H_z\left(i-\tfrac{1}{2}, j+\tfrac{1}{2}, k\right) - H_z\left(i+\tfrac{1}{2}, j+\tfrac{1}{2}, k\right)\right]\Delta_z \\ & + \left[H_x\left(i, j+\tfrac{1}{2}, k+\tfrac{1}{2}\right) - H_x\left(i, j+\tfrac{1}{2}, k-\tfrac{1}{2}\right)\right]\Delta_x \end{aligned} \tag{3}$$

By integrating the electric field along the air-ground interface from the computational domain boundary (point E of Fig. 1) to the lifting line, the transient voltage V_t can be obtained

$$V_t = \sum_{j=N_l}^{N_e} V_j = -\sum_{j=N_l}^{N_e} E_j \Delta s_j \tag{4}$$

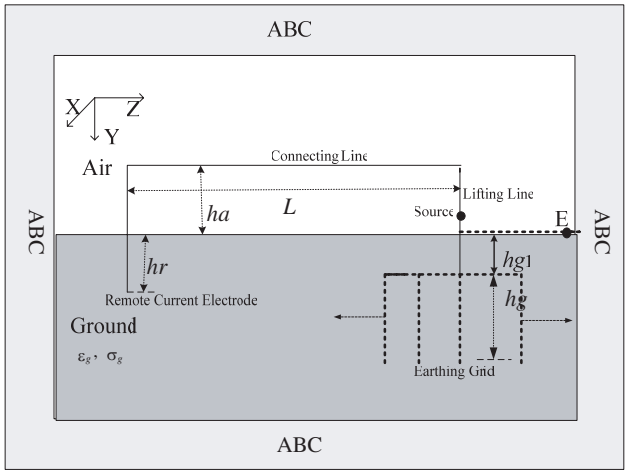

Figure 1. The TGR calculation model, where $hg_1 = 1$ m, $ha = 1$ m.

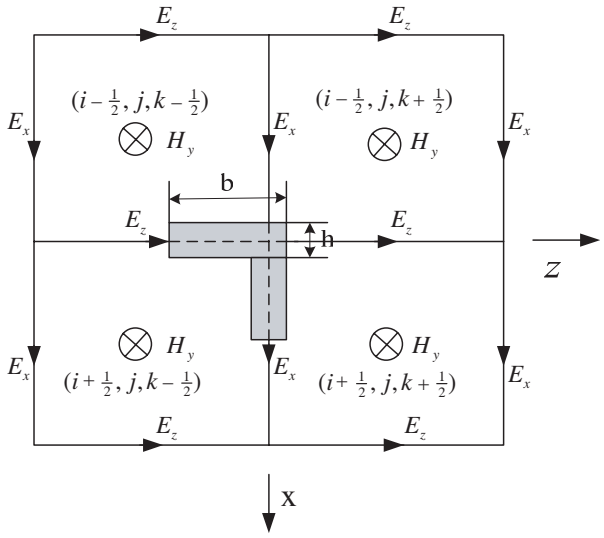

Figure 2. Typical mesh for the magnetic field component H_y near the angle iron earthing conductor, where $h = 0.5\,\text{cm}$, $b = 5\,\text{cm}$.

where N_l and N_e are FDTD mesh indexes of the point of the lifting line entering ground and the point E of Fig. 1. respectively.

2.2. Modeling of the Earthing Conductor

The dimensions of the conductor in the engineering practice maybe quite small compared with the whole TGR calculation domain. For example, the depth of the earthing conductor angle iron is 0.5 cm, while the FDTD computational domain is 4.4 m × 6.8 m × 89 m. Therefore, the coarse FDTD algorithm in [20] is used to reduce the memory usage.

Based on the Yee's mesh, the typical FDTD mesh for modeling the magnetic field near the earthing conductor is shown in Fig. 2. The magnitude of each looping $\vec{H}$ component and radial $\vec{E}$ component are assumed to vary as $1/\sqrt{r}$, where r is the radial distance from the metal edge to the field point.

For the field components in the forth quadrant of Fig. 5, the field variation near the conductor can be expressed as

$$\begin{cases} E_x(x, j\Delta_y, k\Delta_z) = E_x\left(\left(i+\frac{1}{2}\right)\Delta_x, j\Delta_y, k\Delta_z\right)\sqrt{\frac{\Delta_x/2-h/2}{x-(i\Delta_x+h/2)}} \\ E_z(i\Delta_x, j\Delta_y, z) = E_z\left(i\Delta_x, j\Delta_y, \left(k+\frac{1}{2}\right)\Delta_z\right)\sqrt{\frac{\Delta_z/2-(b-h/2)}{z-(k\Delta_z+b-h/2)}} \end{cases} \quad (5)$$

Then the time-stepping equation can be derived by applying the

Faraday's Law with the field variation (5) to the forth quadrant loop

$$H_y^{n+\frac{1}{2}}\left(i+\tfrac{1}{2},j,k+\tfrac{1}{2}\right)=H_y^{n-\frac{1}{2}}\left(i+\tfrac{1}{2},j,k+\tfrac{1}{2}\right)+\frac{\Delta t}{\mu_0 S}\left[E_z^n\left(i+1,j,k+\tfrac{1}{2}\right)\Delta_z\right.$$
$$\left.-E_z^n\left(i,j,k+\tfrac{1}{2}\right)l_{Ez}-E_x^n\left(i+\tfrac{1}{2},j,k+1\right)\Delta_x+E_x^n\left(i+\tfrac{1}{2},j,k\right)l_{Ex}\right] \quad (6)$$

where

$$S = [\Delta_x\Delta_z-(b-h/2)h/2] \quad (7)$$
$$l_{Ez} = 2\sqrt{(\Delta_z/2-h/2)(\Delta_z-h/2)} \quad (8)$$
$$l_{Ex} = 2\sqrt{(\Delta_x/2-(b-h/2))(\Delta_x-(b-h/2))} \quad (9)$$

For the field components near the other conductor interfaces, similar formalisms can be used to define the earthing conductor.

2.3. Selection of the Absorbing Boundary Conditions

The perfectly matched layer (PML) [28] is always used to truncate the computational domain, but it suffers from late-time reflection when terminating highly elongated lattices or when simulating fields with very long time-signatures. However, the Modified PML (MPML) has been proved to be more efficient absorbing the transient waves than the PML [29]. Additionally, the convolution PML (CPML) [21, 22] is highly absorptive of evanescent modes. In this part, the performance of the MPML and the CPML are checked in the TGR analysis. To analyze the performance of the two PML conditions, the computational

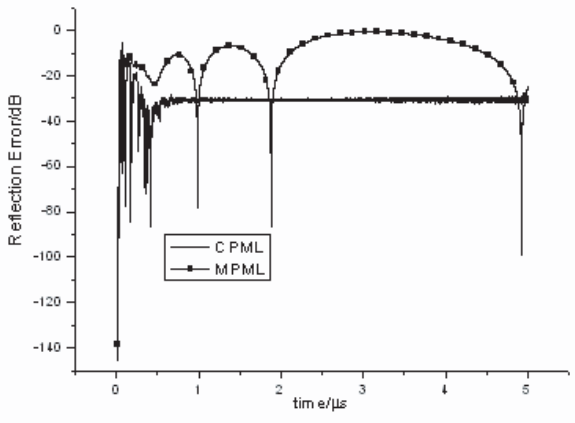

Figure 3. Reflection error in the electric field intensity relative to the field's transient amplitude versus time.

model in Fig. 1 is used, and the reflection error is computed by

$$R_{\mathrm{dB}} = 20\log_{10}\frac{\left|\psi_x^{\mathrm{ref}}(t) - \psi_x^{T}(t)\right|}{\max\left|\psi_x^{\mathrm{ref}}(t)\right|} \tag{10}$$

where $\psi_x^T(t)$ represents the field computed in the test domain and $\psi_x^{\mathrm{ref}}(t)$ is the reference field computed using the larger domain.

The reflection error brought about by the MPML and CPML are graphed in Fig. 3. It is clear that the late-time reflection error brought about by the CPML is much smaller than the MPML. Furthermore, the CPML can provide significant memory savings when computing the wave interaction of elongated structures, sharp corners, or low-frequency excitations. Therefore, in the following analysis, a 8-cell-thick CPML is used to truncate the TGR computational domain.

2.4. Introduction of the Parallel Implementation

Parallel FDTD is a kind of algorithm that the computational domain is divided into several sub-domains and each node only handle for the corresponding sub-domain calculation [23–27]. Therefore, the requirement of the computational storage and time is reduced several times.

Initially, domain decomposition method is one of numerical methods of solving partial differential equations, which is highly suitable for parallel computation [27]. Because of its special feature of involving only the nearest-neighbour interactions when the fields are updated at each time-step, the FDTD is very suitable for a distributed computing implementation. The FDTD modeling of the TGR in this paper is highly elongated, therefore the one-dimensional parallel FDTD division is used in this paper.

The Message Passing Interface (MPI) is a standard specification of a set of libraries call for passing messages between computers interconnected via a data communication network. The MPI standard defines interfaces to two languages, C and FORTRAN, and FORTRAN95 is used in the programming in this paper.

According to the domain decomposition method mentioned above, the original problem is divided into several sub-domains in terms of the features of the problem. Each sub-domain is treated as a process, and MPI connects these processes together.

To approve the efficiency of the proposed parallel implementation method, the TGR given by the serial FDTD simulation are compared with that given by the parallel FDTD simulation. The problem of Fig. 1 is computed, where a line-up earthing grid with $n = 3$ is set as the grounding conductor.

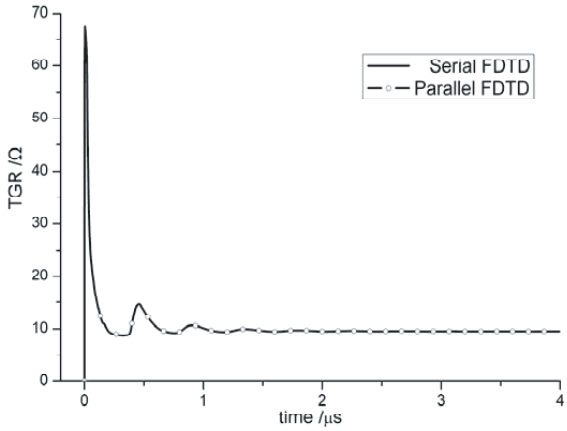

Figure 4. Comparison of the TGR between serial FDTD and parallel FDTD.

When parallel implementation is used, the computation domain is divided along the z-axis because of its high data exchange efficiency and the property of computation model. Both the serial FDTD and parallel FDTD (4 PC nodes) are used to model the problem, and the TGR is graphed in Fig. 4. It can be seen that the parallel FDTD gives the same result as the serial FDTD, thus it can be concluded that the strategy adopted here is feasible.

3. NUMERICAL ANALYSIS OF THE TGR

By using the artifices above, the TGR of large and complex grounding systems can be computed with the FDTD method. To find the optimized program for the grounding systems, the field propagation of the grounding system is analyzed firstly. Secondly, the effect of the earthing conductor number on the TGR is tested. Thirdly, the topology effect on the TGR is analyzed. Fourthly, the buried depth effect on the TGR is tested. Lastly, the TGR is computed with different ground permittivity and conductivity.

3.1. Transient Analysis of the Field Propagation near the Grounding System

To analyze the transient response of the grounding system, it is needed to have a view on the field propagation near the conductors. From the analysis of the time-varied field distribution, the conclusion on the effective conductor length can be easily explained.

In this part, a single rectangular column conductor with the dimension 0.4 m × 0.4 m × 2.5 m is adopted, and the PEC boundary is used to introduce the conductor. Cubic FDTD cell is used and the cell dimension is $\Delta = 0.1$ m, resulting in a $60 \times 84 \times 636$ cells computational domain. Fig. 5 graphs the TGR of the grounding system. It can be seen that the peak value occurs at the time $t_1 = 0.00588$ μs, while the sub-peak value occurs at $t_3 = 0.291$ μs, and after the time $t_4 = 1.5$ μs the TGR tends to be constant.

The distributions of the electric field component E_x at the time t_1, t_3, t_4 are shown in Figs. 6(a), (c) and (d) respectively, where the field distribution at $t_2 = 0.0588$ μs is also included as a reference. From the these graphs, the field propagation phases can be obtained.

(a) It can be seen that from Fig. 6(a) that the electromagnetic field propagates to the limited area very close to the source point, which is 2.8 m above the ground and 3.6 m below the ground, and 2.8 m around the earthing conductor.

(b) From Figs. 6(b) and (c), it can be seen that the electromagnetic field propagates to the nearby areas as the time marching, but the propagation is mainly through the conductor, and a reflection occurs at the air-ground interface.

(c) From Fig. 6(d), it is clear that the electromagnetic field achieves the quasi-static distribution, and the field distributes symmetrically near the conductor, and the TGR becomes constant.

Therefore, it can be concluded that the part of the conductor, which is beyond the efficient length (5.6 m for the horizontal conductor and 3.6 m for the vertical conductor), has limited effect on reducing

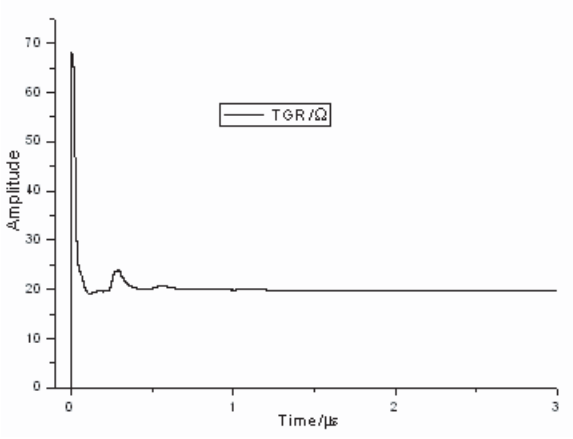

Figure 5. The TGR of the grounding system.

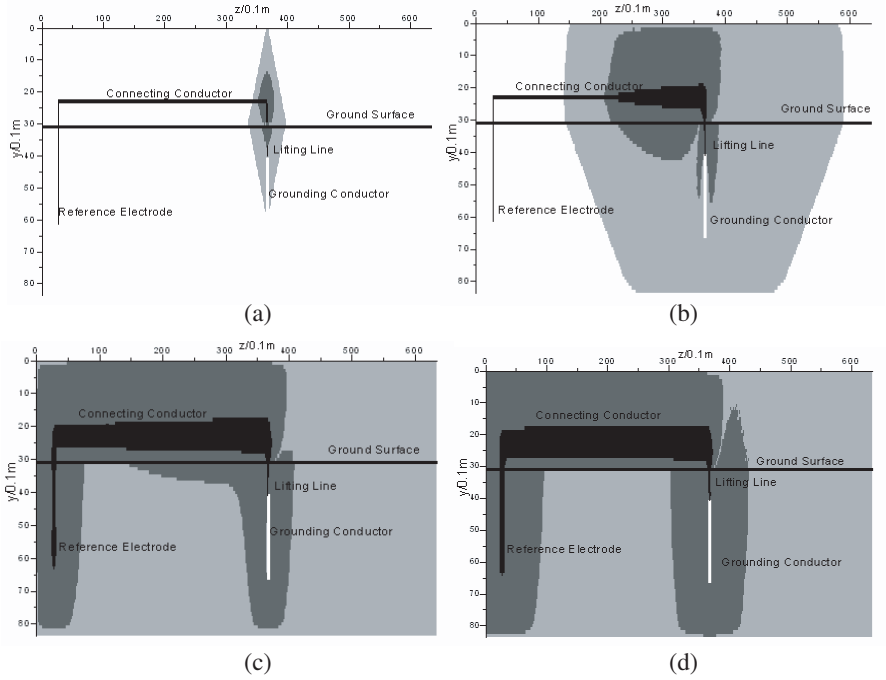

Figure 6. The distribution of electric field component E_x at different times, where the shade of the colure represent the value of the electromagnetic field as below.

white: $0\,\mathrm{V/m}$

undertone gray: $0\,\mathrm{V/m} \sim 60.95\,\mathrm{V/m}$

fuscous gray: $60.95\,\mathrm{V/m} \sim 2.82 \times 10^4\,\mathrm{V/m}$

black: $\geq 2.82 \times 10^4\,\mathrm{V/m}$

the TGR peak value. It is worth to note that the efficient length is given at the conditions that $\sigma = 0.004\,\mathrm{S/m}$, $\varepsilon_r = 9$, and the maximum frequency of the source is 10 MHz.

3.2. The Earthing Conductor Number on the TGR

According to the Type A arrangement in IEC 62305-3 [30], the grounding system is as shown in Fig. 7, where the dimension is also shown. The vertical conductor is 2.5 m in length, and the angle irons are set to be 5 m from the other. The earthing conductor is angle iron, whose size is the same as that in Fig. 2. The computational domain is enlarged in the z direction, resulting in a 4.4 m $\times$ 6.8 m $\times$ 2009.0 m

computation domain.

To analyze the earthing conductor number effect on the TGR, the number of the vertical conductor n varies from 1 to 401. The TGR of the grounding systems composed of n vertical conductors are calculated and the TGR are shown in Fig. 8.

From Fig. 8(a), it can be seen that the constant resistance decreases as the number of the vertical n increases. However, when the number of vertical grounding rods increases to a certain number ($n > 5$), the constant resistance does not decrease remarkably.

Figure 8(b) graphs the TGR of the first 0.1 μs, and it is clear that the peak value of the TGR of the grounding systems is in coincident with each other at the time $0 \sim 0.02$ μs, though the number of vertical conductors are varied.

From the analysis above, it can be seen that increase of the conductor number can not decrease the peak TGR value, but can decrease the constant resistance.

3.3. The Topology Structure Effect on the TGR

In this section, the TGR of different topology structures (line-set and cross-set) with the same total conductor length are analyzed, as shown in Fig. 9. The transient behavior of the two grounding systems is shown in Fig. 10. It can be seen that the two topology structures have the same peak TGR value and the TGR of the cross-set structure decreases at a higher speed than the line-set one. Additionally, the constant resistance of the line-set structure is 6.8 Ω, compared with 9.0 Ω for the cross-set structure.

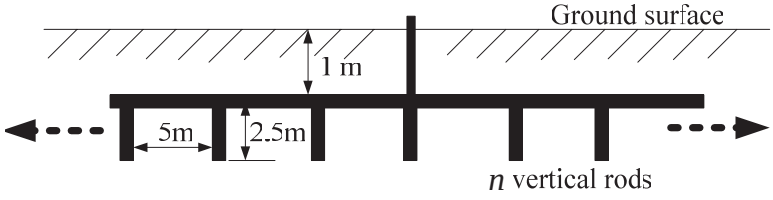

Figure 7. A lineup earthing grid, where the Both the horizontal and vertical grounding conductor are angle iron with figuration shown in Fig. 2.

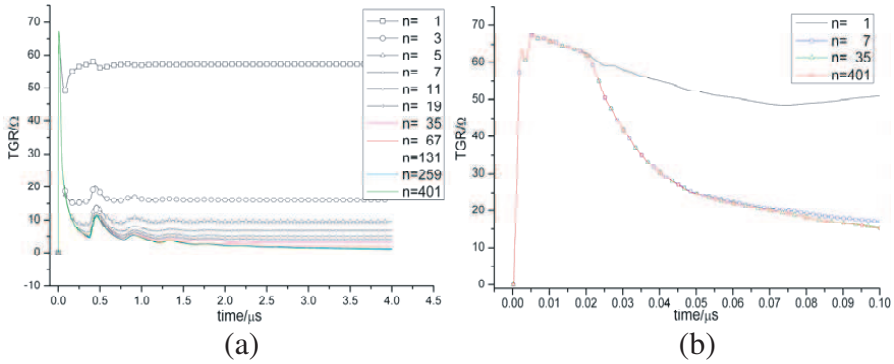

Figure 8. The TGR of the grounding systems with varied numbers of vertical conductors: (a) TGR of 4.0 μs, (b) TGR of the first 0.1 μs.

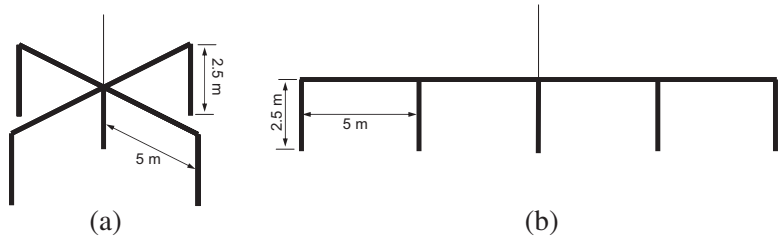

Figure 9. The two different topology structure with the same total conductor length. (a) Cross-set system. (b) Line-set system.

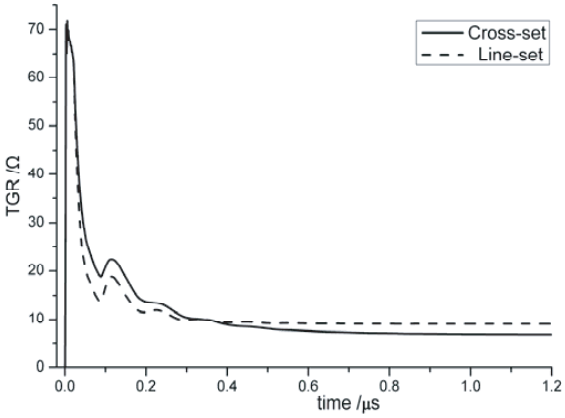

Figure 10. The TGR of the two different topology structures.

3.4. The Buried Depth Effect on the TGR

In this part, the cross-set grounding system as shown Fig. 10(a) is buried at different depth, and the TGR of these conditions are

monitored, as shown in Fig. 11. It is clear that the three buried depth have the same TGR peak value.

To numerically dedicate the TGR lasting time, the half-wave time is introduced, which is the time between the two points where the TGR value is half of its peak value at the increasing and decreasing parts. For example, the peak TGR value for the 2.0 m buried grounding system is 71.86 Ω, the time when the TGR reaches 35.93 Ω at the increasing part is 1.83 μs, and the time when the TGR reaches 35.93 Ω at the decreasing part is 69.17 μs. Thus, the half-wave time can be derived from subtracting 1.83 from 69.17, which is 67.34 μs.

By using the same artifice, the half-wave time at other buried depth can be obtained, as shown in Table 1, where the constant resistance is also listed. We can see that the TGR lasting time increases dramatically as the buried depth increases, while the deeper buried grounding system leads to a lower constant resistance.

3.5. The Ground Parameter Effect on the TGR

In this section, the TGR at varied ground parameters are calculated. Firstly, the ground conductivity varies from 0.004 S/m to 0.1 S/m when

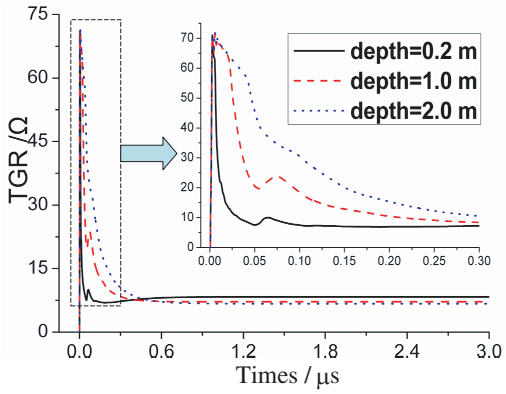

Figure 11. The TGR of the grounding system at three different buried depth.

Table 1. Half-wave time and constant resistance at different buried depth.

Buried depth (m)	0.2	1.0	2.0
Half-wave time (μs)	6.0	31.7	67.3
Constant resistance (Ω)	8.3	7.2	6.7

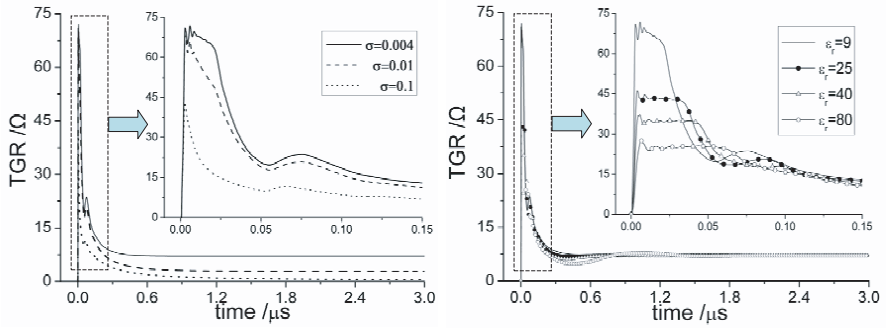

Figure 12. The ground permittivity and conductivity effect on the TGR. (a) Varied conductivity when $\varepsilon_r = 9$. (b) Varied permittivity when $\sigma = 0.004\,\mathrm{S/m}$.

Table 2. Peak TGR value and constant resistance at varied ground parameters.

	1	2	3	4	5	6
ε_r	9.0	9.0	9.0	25.0	40	80
σ (S/m)	0.004	0.01	0.1	0.004	0.004	0.004
Peak TGR value (Ω)	71.86	68.32	43.18	46.23	37.16	27.54
Constant resistance (Ω)	7.16	2.84	0.46	7.16	7.17	7.19

the relative permittivity is 9. Additionally, the relative permittivity of the ground is set to be varied from 9 to 80 when the ground conductivity is 0.004.

Figure 12 graphs the TGR of the grounding system at varied ground parameters, while Table 2 shows the peak TGR value and the constant resistance. Fig. 12(a) shows that both the peak TGR value and the constant resistance decrease dramatically as the conductivity increases. From Fig. 12(b), it can be seen that the peak TGR value decreases when the relative permittivity increases from 9 to 80, while the constant resistance is almost the same. Additionally, from Fig. 12(b) it is clear that increase the relative permittivity will result in a longer TGR lasting time.

It can be seen from Table 2 that the increase of both the permittivity and the conductivity can decrease the peak TGR value. However, increasing the relative permittivity will result in a longer TGR lasting time, while the increase of the ground conductivity can both decrease the peak value and the TGR lasting time. Furthermore, the constant resistance is mainly determined the ground

conductor. The constant resistance is nearly the same when the relative permittivity is 9.0 and 80 respectively, while the constant resistance decreases dramatically from 7.16 Ω to 0.46 Ω as the conductivity increases.

From the analysis above, some useful conclusion can be derived, which may help the TGR grounding system design.

Firstly, the electromagnetic field propagates to a limited area very close to the source point when the TGR reaches its peak value, and the conductor that is beyond this efficient length will has limited effect on the peak TGR value.

Secondly, increasing the electrode number cannot decrease the peak value of the TGR, but the constant resistance of the grounding system decreases dramatically as the number of the electrodes increases when the number is less than 5.

Thirdly, the line-set grounding system has a shorter TGR lasting time, while the cross-set system has a lower constant resistance.

Fourthly, the TGR lasting time increases and the constant resistance decreases as the buried depth increases.

Lastly, increase of the conductivity can both decrease the peak TGR value and constant resistance of the grounding system, while increase the permittivity will result in a longer TGR lasting time, while increase the permittivity will decrease the peak TGR value but result in a longer TGR lasting time.

4. CONCLUSIONS

In this work, a new method has been proposed for the FDTD analysis of the TGR of the lightning protection grounding system. The coarse FDTD grid is used to simulate the earthing conductor, and the CPML is used to truncate the computational domain for its good performance in absorbing the late-time reflection of the TGR analysis. The parallel implement is verified to be an efficient way of overcoming the memory limit of the serial processor in the TGR analysis.

With the proposed model, the parameters of the grounding system are altered to find the optimized program. Firstly, the field propagation of the grounding system is analyzed, and it is found that the electromagnetic field propagates to the limited area very close to the source point when the TGR reaches its peak value, and the conductor that is beyond this efficient length will has limited effect on the peak TGR value. Secondly, the effect of the earthing conductor number on the TGR is tested, and it is found that increasing the conductor number could not decrease the peak value of the TGR, but the constant resistance decreases dramatically when it is less than

5. Thirdly, the TGR of different topology structures are tested, and it is found that the line-set grounding system has a shorter TGR lasting time, while the cross-set system has a lower constant resistance. Fourthly, the buried depth effect on the TGR is tested, and it is found that the TGR lasting time increases and the constant resistance decreases as the buried depth increases. Lastly, the TGR is computed at different ground parameters, and it is concluded that increase of the conductivity can both decrease the peak TGR value and constant resistance of the grounding system, while increase the permittivity will decrease the peak TGR value but result in a longer TGR lasting time.

The conclusions derived in this paper would be useful in the grounding system design.

REFERENCES

1. Grcev, L. and F. Dawalibi, "An electromagnetic model for transients in grounding systems," *IEEE Trans. on Power Delivery*, Vol. 5, No. 4, 1773–1780, November 1990.
2. Grcev, L., "Computer analysis of transient voltage in large grounding systems," *IEEE Trans. on Power Delivery*, Vol. 11, No. 2, 815–823, April 1996.
3. Grcev, L. and D. Hristov, "More accurate modeling of earthing systems transient behaviour," *15th International Telecommunications Energy Conference, INTELEC*, Vol. 2, 167–173, Paris, France, 1993.
4. Visacro, S. F., "Modeling of earthing systems for lightning protection applications, including propagation effects," *ICLP*, Berlin, Germany, 1992.
5. Johny, M., "Recommendation for grounding systems in lightning protection systems," *ISEPQ,* Vol 31, Sup. 2, 5–10, Asuncion, Paraguay, October 2011.
6. Izadi, M., M. Z. A. Ab Kadir, C. Gomes, and W. F. Wan Ahmad, "An analytical second-FDTD method for evaluation of electric and magnetic fields at intermediate distances from lightning channel," *Progress In Electromagnetics Research*, Vol. 110, 329–352, 2010.
7. Gomes, C. and Z. A. Zb. Kadir, "Protection of naval systems against electromagnetic effects due to lightning," *Progress In Electromagnetics Research*, Vol. 113, 333–349, 2011.
8. Izadi, M., M. Z. A. Ab Kadir, and C. Gomes, "Evaluation of electromagnetic fields associated with inclined lightning channel using second order FDTD-hybrid methods," *Progress In Electromagnetics Research*, Vol. 117, 209–236, 2011.

9. Lee, K. H., I. Ahmed, R. S. M. Goh, E. H. Khoo, E. P. Li, and T. G. G. Hung, "Implementation of the FDTD method based on lorentz-drude dispersive model on GPU for plasmonics applications," *Progress In Electromagnetics Research*, Vol. 116, 441–456, 2011.
10. Kong, Y.-D. and Q.-X. Chu, "Reduction of numerical dispersion of the six-stages split-step unconditional-stable FDTD method with controlling parameters," *Progress In Electromagnetics Research*, Vol. 122, 175–196, 2012.
11. Sirenko, K., "An FFT-accelerated FDTD scheme with exact absorbing conditions for characterizing axially symmetric resonant structures," *Progress In Electromagnetics Research*, Vol. 111, 331–364, 2011.
12. Xiao, S.-Q., Z. H. Shao, and B.-Z. Wang, "Application of the improved matrix type FDTD method for active antenna analysis," *Progress In Electromagnetics Research*, Vol. 100, 245–263, 2010.
13. Cao, D.-A. and Q.-X. Chu, "FDTD analysis of chiral discontinuities in waveguides," *Progress In Electromagnetics Research Letters*, Vol. 20, 19–26, 2011.
14. Ai, X., Y. Han, C. Y. Li, and X.-W. Shi, "Analysis of dispersion relation of piecewise linear recursive convolution FDTD method for space-varying plasma," *Progress In Electromagnetics Research Letters*, Vol. 22, 83–93, 2011.
15. Silva, A. O., R. Bertholdo, M. G. Schiavetto, B.-H. V. Borges, S. J. L. Ribeiro, Y. Messaddeq, and M. A. Romero, "Comparative analysis between experimental characterization results and numerical FDTD modeling of self-assembled photonic crystals," *Progress In Electromagnetics Research B*, Vol. 23, 329–342, 2010.
16. Xu, K., Z. Fan, D.-Z. Ding, and R.-S. Chen, "GPU accelerated unconditionally stable Crank-Nicolson FDTD method for the analysis of three-dimensional microwave circuits," *Progress In Electromagnetics Research*, Vol. 102, 381–395, 2010.
17. Lu, J., Z. Fan, D.-Z. Ding, and R.-S. Chen, "FDTD method investigation on the polarimetric scattering from 2-D rough surface," *Progress In Electromagnetics Research*, Vol. 101, 173–188, 2010.
18. Tanabe, K., "Novel method for analyzing dynamic behavior of grounding systems based on the finite-difference time-domain method," *IEEE Power Engineering Review*, Vol. 21, 55–57, 2001.
19. Tannus, T. E., R. O. dos Santos, R. M. S. de Oliveira, and C. L. da Silva Souza, "Transient analysis of parameters governing grounding systems by the FDTD method," *IEEE Latin America*

Transactions, Vol. 4, No. 1, 55–61, March 2006.

20. Xiong, R., B. Chen, Y.-F. Mao, W. Deng, Q. Wu, and Y.-Y. Qiu, "FDTD modeling of the earthing conductor in the transient grounding resistance analysis," *IEEE Antennas and Wireless Propagat. Lett.*, Vol. 35, 1248–1257, August 2012.
21. Roden, J. A. and S. D. Gedney, "Convolution PML (CPML): An efficient FDTD implementation of the CFS-PML for arbitrary media," *Microwave and Optical Technology Lett.*, Vol. 27, 334–339, 2000.
22. Mao, Y.-F., B. Chen, H.-Q. Liu, J.-L. Xia, and J.-Z. Tang, "A hybrid implicit-explicit spectral FDTD scheme for the oblique incidence programs on periodic structures," *Progress In Electromagnetics Research*, Vol. 128, 153–170, 2012.
23. Lei, J. Z., C. H. Liang, and Y. Zhang, "Study on shielding effectiveness of metallic cavities with apertures by combining parallel FDTD method with windowing technique," *Progress In Electromagnetics Research*, Vol. 74, 85–112, 2007.
24. Vaccari, A., A. Cala' Lesina, L. Cristoforetti, and R. Pontalti, "Parallel implementation of a 3-D subgridding FDTD algorithm for large simulation," *Progress In Electromagnetics Research*, Vol. 120, 263–292, 2011.
25. Taboada, J. M., M. G. Araujo, J. M. Bertolo, L. Landesa, F. Obelleiro, and J. L. Rodriguez, "MLFMA-FFT parallel algorithm for the solution of large-scale problems in electromagnetics," *Progress In Electromagnetics Research*, Vol. 105, 15–30, 2010.
26. Ergul, O., "Parallel implementation of MLFMA for homgeneous objects with various material properties," *Progress In Electromagnetics Research*, Vol. 121, 505–520, 2010.
27. Yang, D., J. Xiong, C. Liao, and L. Jen, "A parallel FDTD algorithm based on domain decomposition method using the MPI library," *PDCAT's*, 730–733, 2003.
28. Berenger, J. P., "A perfectly matched layer for the absorption of the electromagnetic waves," *J. Comput. Phys.*, 185–200, 1994.
29. Chen B., D. G. Fang, and B. H. Zhou, "Modified Berenger PML absorbing boundary condition for FD-TD meshes," *IEEE Microwave and Guided Wave Letters*, Vol. 5, No. 11, 399–401, November 1995.
30. IEC 62305-3. ed.2.0, *Protection Against Lightning — Part 3: Physical Damage to Structures and Life Hazard*, 2004.